2024 IEEE/SICE International Symposium on System Integration (SII)
January 8-11, 2024. Ha Long, Vietnam

Modeling and Identification of the Dehydration Process in a $CaO/Ca(OH)_2$-based Heat Storage System*

Anja Rentz[1], Viktor Kühl[2], Matthias Schmidt[2], Marc Linder[3], Oliver Sawodny[1], Michael Böhm[1]

Abstract— **Thermochemical energy storage systems are considered a loss free, environmentally friendly solution for storage of renewable energy. This work focuses on a specific application based on $CaO/Ca(OH)_2$ for heat storage. During the endothermic dehydration of $Ca(OH)_2$, heat is stored in the chemical bonds. By bringing CaO and H_2O together in the exothermic hydration process, the stored heat is recovered.**

In this work, we set up a mathematical model to describe the dehydration process. The model covers the reaction driven by heaters in the reactor and the mass flow of gaseous water along a pressure gradient to a heat exchanger, where it condenses. Working towards model based control of the reactor system, the model equations are derived using enthalpy and mass balances as well as reaction kinetics. This yields dynamic equations for the reactor temperature, the water mass in the condenser and the conversion.

Three unknown parameters related to heat transfer are identified via an optimization problem. For three data sets we apply a cross validation scheme, where two data sets are used for identification and the third one for model validation. All combinations of data sets in the cross validation were investigated and evaluated with the root mean square error and the qualitative model behavior.

Although the identification of a distinct, globally optimal parameter set is challenging, the best parameter set is identified and can be used for future investigations and controller design.

I. INTRODUCTION

The operation of buildings accounts for 30% of global final energy consumption [1], with operational CO_2 emissions of around 10Gt in 2021 [2]. Almost half of the energy demand for buildings is associated to space and water heating, with a share of over 60% of heating energy demand being covered by fossil fuels [3]. Research for efficient and renewable energy technology has been intensified for the last years, as the importance of efficient and low-carbon heating technologies will continue to grow.

A straightforward solution for reducing CO_2 emissions would be to electrify the heating system with electricity from renewable sources. However, there is a gap between renewable production and building heating demand, as heating is required in winter, while solar and wind energy peak in summer and the transitional seasons.

Thermochemical energy storage is considered to have high potential closing this supply demand gap, as energy is stored loss free in the chemical bonds over time. One promising system realization is based on the reversible reaction of solid CaO and liquid or gaseous H_2O to solid $Ca(OH)_2$

$$\mathrm{CaO} + \mathrm{H_2O} \rightleftharpoons \mathrm{Ca(OH)_2} + \Delta H, \tag{1}$$

where ΔH is the reaction enthalpy depending on the state of water. The material and reaction properties have been studied in detail in [4], [5], [6], [7].

Energy stored during the endothermic dehydration is recovered when needed in the exothermic hydration process. Thereby, waste heat from the endothermic charging process can be recovered for hot water use or heating purposes. The cheap and non-toxic materials can be stored in between cycles in simple containers at ambient conditions [8].

An intuitive operation principle charges the system with surplus electrical energy from renewable sources, and discharges in winter when heating demand is high. Adjusting pressure and temperature conditions during the processes while fulfilling requirements for the heating and warm water system is technically challenging. Model-based control offers an approach to meet both reaction kinetics and system specific requirements.

Having already modeled the hydration process [9], we now consider the dehydration process in this work, to generate a full model description of the system and enabling further work on control.

At first, batch reactor models from the literature [10], [11], [12] were reviewed. For our application, however, the model has to be extended for semi-batch operation.

For this type of thermal energy storage, a fixed bed is a common choice because of its simplicity. This also has the advantage that it can be described by a differential equation of space and time, yielding a distributed model, cf. [13], [14]. As our reactor contains a fluidized bed for improved heat transfer, this description can not be used and the governing model equations only depend on time.

The existing 1D-model for a chemical heat pump based on $CaO/Ca(OH)_2$ in [15] was thoroughly reviewed, however, the authors also consider a fixed bed reactor. Furthermore, the authors do not provide a description of the mass flow exiting the reactor to the condenser.

Our model includes the mass flow and we proceed with parameter identification, since not all parameters can be deduced from literature. Therefore the main contribution of

*Funded by the Deutsche Forschungsgemeinschaft (DFG, German Research Foundation) - Project-ID 279064222 - SFB 1244, A05 and the European Funds for Regional Development (EFRE Program) within the I-TESS project Project-ID EFRE-0801821.

[1]Anja Rentz, Oliver Sawodny and Michael Böhm are with the Institute for System Dynamics, University of Stuttgart, 70174 Stuttgart, Germany {rentz,sawodny,boehm}@isys.uni-stuttgart.de

[2]Viktor Kühl and Matthias Schmidt are with the German Aerospace Center (DLR), Linder Höhe, 51147 Cologne, Germany {Viktor.Kuehl,Matthias.Schmidt}@dlr.de

[3]Marc Linder is with the German Aerospace Center (DLR), Pfaffenwaldring 38-40, 70569 Stuttgart, Germany Marc.Linder@dlr.de

2024 IEEE/SICE International Symposium on System Integration (SII) | 979-8-3503-1207-2/24/$31.00 ©2024 IEEE | DOI: 10.1109/SII58957.2024.10417332

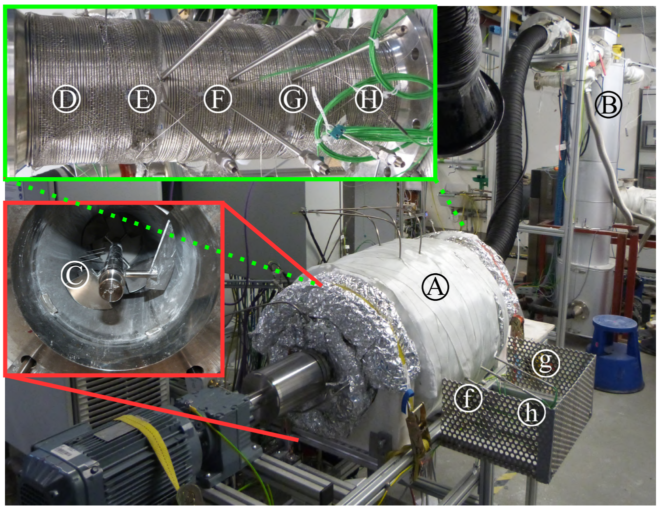

Fig. 1: Thermochemical reactor in the laboratory setup. The plowshare mixing tool Ⓒ is displayed in the plot on the left (red). The heating wires Ⓓ - Ⓗ around the reactor tube are shown in the top left plot (green). Source: [16].

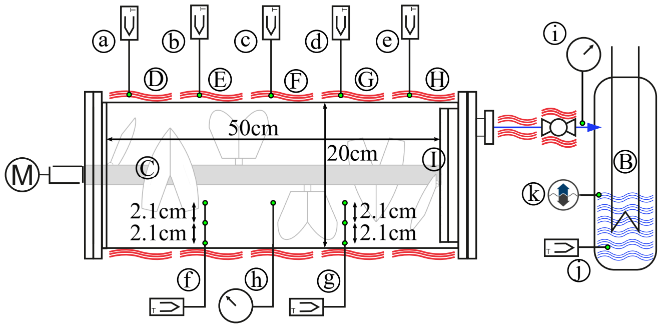

Fig. 2: Side view of the reactor system for dehydration with the reactor on the left and the condenser Ⓑ.

this work is the full model of the dehydration process in our fluidized-bed reactor, identifying parameters with multiple data sets.

This work is structured as follows. Section II briefly introduces the experimental setup. In Section III, the system dynamics are derived, followed by Section IV, where the parameter identification optimization problem is set up. Section V presents the identification results. Finally, Section VI closes this work with a conclusion and outlook.

II. System description

The reactor principle is described in detail in [16]. A mechanically fluidized bed reactor is used to overcome the low thermal conductivity of the materials $CaO/Ca(OH)_2$. Figures 1 and 2 show the reactor system in the laboratory setup and the sensor system. The following section will provide further details on the setup.

A. Test Bench

The test bench in closed operation consists of the reactor Ⓐ and a system to condition the gas atmosphere. A vacuum pump removes initial atmospheres and inert gases. Due to the low pressure, water in the condenser Ⓑ evaporates and creates a steam atmosphere. An oil thermostatic bath brings the condenser to a desired temperature.

The plowshare mixing tool Ⓒ creates the fluidized bed in the reactor. It is connected to a motor with a nominal power of $1.5\,\mathrm{kW}$ and a maximum rotational speed of $292\,\mathrm{rpm}$.

Five heating wires Ⓓ - Ⓗ with an effective power of about $2.7\,\mathrm{kW}$ heat up the reactor, starting the reaction. One thermocouple per heating wire ⓐ - ⓔ measures the respective heater temperature. Two three-point thermocouples ⓕ, ⓖ measure the bulk temperature in the reactor inner, having a diameter of $4\,\mathrm{mm}$.

On the outside, the reactor is insulated by a $0.15\,\mathrm{m}$ thick insulation wool layer to minimize thermal losses.

A twilled weave filter material with a filter fineness of $5\,\mathrm{\mu m}$ separates the reactor from the gas system on one side. The opposite inner side of the reactor is covered with a $50\,\mathrm{mm}$ thick insulating plate.

The pressure in the reactor and in the condenser is measured with pressure sensors ⓗ and ⓘ, respectively.

The heat exchanger temperature can be set via the oil flowing the tube bundles. The condenser temperature determines evaporation/condensation and therefore the condenser pressure. During experiments, the pressure difference between reactor and condenser drives the mass transport of gaseous water from the reactor through the filter to the condenser, where the gaseous water immediately condenses. The condenser filling level is measured ⓚ. The temperature of the water in the condenser is measured as well ⓙ.

B. Sensors

All thermocouples ⓐ - ⓖ, ⓙ are of type K class 1 with uncertainty of $1.5\,^{\circ}\mathrm{C}$ or $0.4\,\%|\mathrm{T}|$, whereby $|\mathrm{T}|$ is the measurement point temperature. The two pressure sensors ⓗ, ⓘ for reactor and condenser have a range of 0 to $300\,\mathrm{kPa}$ abs. and a maximum error of $\pm 0.6\,\mathrm{kPa}$. The water level is measured by a microwave level sensor ⓚ (uncertainty of $\pm 2\,\mathrm{mm}$ corresponding to $\pm 0.0255\,\mathrm{kg}$). This output is used to monitor the the reaction progress.

C. Material

For the hydration, off the shelf $Ca(OH)_2$ from Rheinkalk GmbH/Lhoist group are used. The manufacturer attests the $Ca(OH)_2$ powder a purity of $95\,\%$, a bulk density of $380\,\mathrm{kg/m^3}$, a mean particle diameter (d_{50}) of $5.1\,\mathrm{\mu m}$ and a specific surface area of $18\,\mathrm{m^2/g}$. To check the initial material composition, a thermogravimetric analysis is carried out for the batch of material used. According to these measurements, the composition of the material is 86.67% $Ca(OH)_2$, 4.43% CaO, 8.90% $CaCO_3$.

D. Experimental Procedure

To ensure equal initial conditions, fresh material is used for each test run and the reactor is completely emptied after each test. For the experiments, a bulk mass of about $5\,\mathrm{kg}$ and rotational speed of $250\,\mathrm{rpm}$ are used.

The reactor and the condenser are separated by a ball valve, which is closed at the beginning of the experiment. The experimental procedure is as follows: 1. Pre-heating up

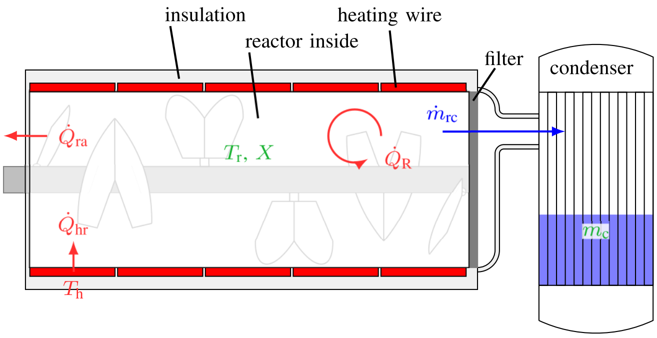

Fig. 3: Model of the reactor during the dehydration, side view.

to around 350 °C. 2. Evacuation of the system, removing inert gases. 3. Further heating until the reactor reaches the desired reaction temperature. At the same time, the condenser temperature is adjusted by setting the temperature of the thermostatic bath to a fixed value. 4. Both reactor and condenser reach a state of equilibrium. 5. The endothermic reaction starts as soon as the connection between reactor and condenser is opened. 6. After a fixed time of 2 h, the experiment is stopped. The heaters are turned off and a valve connecting the reactor to the environment is opened, bringing the reactor back to ambient pressure.

The heater temperatures follow a simple two-level control logic. They provide a constant temperature, until the reactor temperature reaches the desired range for the experiment. If the reactor temperature exceeds a predefined maximum value, the heaters are turned off one by one until the reactor temperature falls back in the desired temperature range. As the controllers operate separately, the heater temperatures are not always equal, resulting in a temperature gradient along the reactor tube. However, the gradient cannot be quantified since the temperature at the measurement points is kept constant by the control.

III. Modeling

This section establishes the reactor model for dehydration. The derivation of the model equations is based on mass and enthalpy balances and reaction kinetics. All effects considered in the modeling are depicted in Fig. 3.

Due to the shovel rotation, we assume the reactor inside to be perfectly mixed. The homogeneous conditions imply uniform temperature and equally distributed materials. The five heating zones are assumed to be homogeneous as well, resulting in a single heater temperature.

The most common symbols are listed in Tab. IV and subscripts in Tab. I. For simplicity and in accordance to our work on the hydration, the reactants are referred to using the subscript 1 for CaO, 2 for H_2O and 3 for $Ca(OH)_2$, as noted in Tab. I.

TABLE I: Subscripts.

Subscript	Description
h	heater
r	reactor
c	condenser
a	ambiance
cn	additional heat capacities and masses
1	CaO
2	H_2O
3	$Ca(OH)_2$

The advancing process is characterized by the conversion X, which is obtained from [5] and writes as

$$\dot{X} = \begin{cases} 1.94 \cdot 10^{12} \exp\left(\frac{-187.88 \cdot 10^3}{R(T_{\mathrm{r}}+273.15)}\right) & \\ \left(1 - \frac{p_{\mathrm{r}}}{p_{\mathrm{eq}}}\right)^3 (1-X), & 0 \leq X < 0.2, \\ 8.96 \cdot 10^9 \exp\left(\frac{-162.62 \cdot 10^3}{R(T_{\mathrm{r}}+273.15)}\right) & \\ \left(1 - \frac{p_{\mathrm{r}}}{p_{\mathrm{eq}}}\right)^3 2(1-X)^{0.5}, & 0.2 \leq X \leq 1, \\ 0, & \text{else}, \end{cases} \tag{2}$$

with universal gas constant R, reactor temperature T_{r}, reactor pressure p_{r} and reactor equilibrium pressure p_{eq}.

The equilibrium pressure in Pa is taken from literature [5] and depends on the reactor temperature

$$p_{\mathrm{eq}} = 10^5 \exp\left(\frac{-12845}{T_{\mathrm{r}}} + 16.508\right). \tag{3}$$

The conversion is a normalized amount of substance. Its relation to the amount of $Ca(OH)_2$ n_3 is

$$X = \frac{n_{30} - n_3(t)}{n_{30}} + X_0, \tag{4}$$

with the initial amount of $Ca(OH)_2$ n_{30} and initial conversion X_0. The reaction rate R_{r}, describing the changes of the amounts of substance, can therefore be deduced from the conversion rate via

$$R_{\mathrm{r}} = n_{30}\dot{X}. \tag{5}$$

The amounts of substance CaO n_1, gaseous water n_2 and $Ca(OH)_2$ n_3 therefore are

$$n_1 = n_{30}\left(X - X_0\right) + n_{10}, \tag{6}$$

$$n_2 = n_{30}\left(X - X_0\right) + n_{20} - \frac{m_{\mathrm{c}} - m_{\mathrm{c0}}}{M_2}, \tag{7}$$

$$n_3 = -n_{30}\left(X - X_0\right) + n_{30} \tag{8}$$

with condenser water mass m_{c}, molar mass of water M_2, initial conditions n_{10}, n_{30} and m_{c0} from measurement and n_{20} from the ideal gas law

$$n_{20} = \frac{p_{\mathrm{r0}} V_{\mathrm{r}}}{R\left(T_{\mathrm{r0}} + 273.15\right)}. \tag{9}$$

In this, p_{r0} is the initial pressure from measurements and T_{r0} the initial reactor temperature, V_{r} is the reactor volume.

The gaseous water in the condenser is assumed to condense immediately, as the temperature is low. The mass flow from the reactor to the condenser is assumed to be proportional to the pressure difference, as experiments suggest. The dynamic of the liquid water mass in the condenser m_{c} is

$$\dot{m}_{\mathrm{c}} = \overbrace{\begin{cases} \eta_{\mathrm{rc}}\left(p_{\mathrm{r}} - p_{\mathrm{c}}\right), & t \geq t_1, \\ 0, & \text{else}. \end{cases}}^{\dot{m}_{\mathrm{rc}}} \tag{10}$$

with proportionality factor η_{rc} and condenser pressure p_{c}. At time t_1, the reactor connection to the condenser is opened.

To compute the pressure in the reactor, the superheated steam is modeled as an ideal gas. The reactor pressure p_r via ideal gas law is

$$p_\mathrm{r} = \frac{R\, n_2\, (T_\mathrm{r} + 273.15)}{V_\mathrm{r}}. \tag{11}$$

For the condenser, it is assumed that the saturation pressure is determined by the measured condenser temperature T_c. The condenser pressure is therefore given by the Magnus formula [17]

$$p_\mathrm{c} = 611.2 \cdot \exp\left(\frac{17.62\, T_\mathrm{c}}{243.12 + T_\mathrm{c}}\right). \tag{12}$$

Under the assumption of constant heat capacity for all materials and substances involved, the enthalpy balance for the reactor can be reformulated as a temperature balance. This yields the following dynamics for the reactor temperature

$$\begin{aligned}\dot{T}_\mathrm{r} = \underbrace{\left(\sum_{i=1}^{n_r} c_{\mathrm{p},i} n_i + c_\mathrm{cn,r}\right)^{-1}}_{①} \Bigg[& \underbrace{\Delta H R_\mathrm{r}}_{\text{heat of reaction}=:\dot{Q}_\mathrm{R}} \\ & \underbrace{+ A_\mathrm{hr} U_\mathrm{hr}\,(T_\mathrm{h} - T_\mathrm{r})}_{\text{heat transfer heater to reactor}=:\dot{Q}_\mathrm{hr}} \quad \underbrace{- A_\mathrm{ra} U_\mathrm{ra}\,(T_\mathrm{r} - T_\mathrm{a})}_{\text{heat loss to ambiance}=:\dot{Q}_\mathrm{ra}} \\ & \underbrace{-\,(c_{\mathrm{p},1} + c_{\mathrm{p},2} - c_{\mathrm{p},3})\, R_\mathrm{r} T_\mathrm{r}}_{②} \Bigg],\end{aligned} \tag{13}$$

with reaction enthalpy $\Delta H = H_{0,3} - H_{0,1} - H_{0,2}$, heater temperature T_h, ambient temperature T_a, heat transfer areas A_hr, A_ra and thermal transmittances U_hr, U_ra, characterizing the heat transfer from heater to reactor and reactor to ambiance respectively, as well as amounts of substance n_i and associated heat capacities $c_{\mathrm{p},i}$, and $n_r = 3$ for the three substances involved. The constant $c_\mathrm{cn,r}$ accounts for additional thermal masses that are not explicitly considered in the modeling, e.g. the plowshare mixing tool. The terms ① and ② originate from the conversion of the enthalpy balance into a temperature balance.

The model of the dehydration process in the reactor system consists of the state equations (2),(10),(13), and has the outputs T_r and m_c directly, p_r from (11). Plugging the algebraic equations (3)-(9) and (12) into the state equations results in a nonlinear system with nonlinear output equation

$$\dot{\boldsymbol{x}} = \boldsymbol{f}(\boldsymbol{x}, \boldsymbol{u}, \boldsymbol{v}),\ \boldsymbol{x}(0) = \boldsymbol{x_0}, \tag{14}$$

$$\boldsymbol{y} = \boldsymbol{g}(\boldsymbol{x}, \boldsymbol{u}), \tag{15}$$

with state $\boldsymbol{x} = [T_\mathrm{r}, m_\mathrm{c}, X]^T \in \mathbb{R}^3$, input $\boldsymbol{u} = T_\mathrm{h} \in \mathbb{R}$, time dependent disturbance $\boldsymbol{v} = [T_\mathrm{c}, T_\mathrm{a}] \in \mathbb{R}^2$, and output $\boldsymbol{y} = [T_\mathrm{r}, m_\mathrm{c}, p_\mathrm{r}]^T \in \mathbb{R}^3$. The initial conditions $T_\mathrm{r0} = T_\mathrm{r}(0)$ and $m_\mathrm{c0} = m_\mathrm{c}(0)$ are obtained from measurements, the initial conversion is $X_0 = X(0) = 0$.

IV. Parameter Identification

Since not all parameters can be measured in the experimental setup, parameter identification is carried out for the remaining parameters. Table V summarizes all model parameters that can be deduced from measurements or directly measured, e.g. heat transfer area, and parameters from literature, e.g. material properties such as the molar heat capacities of the substances involved. The remaining model parameters are summarized in the parameter vector $\boldsymbol{\theta} = [U_\mathrm{hr}, U_\mathrm{ra}, c_\mathrm{cn,r}]^T$ and will be identified.

The identification is carried out with the help of an optimization. For this, data from three dehydration experiments are used. The parameter identification optimization problem writes as

$$\min_{\boldsymbol{\theta}} \sum_{j=1}^{k} \sum_{m=1}^{3} \frac{q_m^2}{N^2} \sum_{i=0}^{N} \left(\frac{y_{m,j,\mathrm{sim}}(i\Delta t, \boldsymbol{\theta}) - y_{m,j,\mathrm{meas},i}}{\bar{y}_{m,\mathrm{meas}}}\right)^2 \tag{16a}$$

$$\text{s.t.}\ \dot{\boldsymbol{x}} = \boldsymbol{f}(\boldsymbol{x}, \boldsymbol{u}, \boldsymbol{v}), \tag{16b}$$

$$\boldsymbol{x}(0) = \boldsymbol{x_0}, \tag{16c}$$

$$\boldsymbol{y}_\mathrm{sim} = \boldsymbol{g}(\boldsymbol{x}, \boldsymbol{u}), \tag{16d}$$

$$\boldsymbol{\theta}_\mathrm{min} \leq \boldsymbol{\theta} \leq \boldsymbol{\theta}_\mathrm{max}. \tag{16e}$$

The cost to be minimized is the quadratic deviation of measurement and simulation for all time steps N, for the three measured outputs and k different data sets. It is possible to identify parameters using all three available data sets ($k = 3$). However, we apply a cross validation scheme, i.e. using two data sets for identification ($k = 2$) and the remaining one for model validation with the identified parameters. The procedure provides direct information on the model quality for data it has not been identified with and is applied for all combinations of data sets.

The division by the average measured output value $\bar{y}_\mathrm{m,meas}$ and the number of time steps N normalizes the optimization cost, while the weighting factors q_m can be adjusted to account for different sensor accuracy or to prioritize modeling accuracy for one of the outputs. The weights are set to $q_1 = 100$, $q_2 = 4000$, $q_3 = 1000$. In this case, because the temperature is distributed throughout the reactor and a gradient due to different heating wire temperatures is possible, we put a lower weight on the the reactor temperature measurement than on the condenser water mass and reactor pressure measurements.

The model outputs $y_{m,j,\mathrm{sim}}(i\Delta t, \boldsymbol{\theta})$ are obtained by simulating the system dynamics with parameters $\boldsymbol{\theta}$, evaluated at time step i with constant step size Δt.

The values $y_{m,j,\mathrm{meas},i}$ are the measured outputs at time step i. For the reactor temperature $y_{1,j,\mathrm{meas},i}$, the values of the six multipoint measurements are averaged. The averaged temperature of the five heating zones serves as heater temperature input T_h for the model.

The parameters are subject to the constraints $\boldsymbol{\theta}_\mathrm{min}$ and $\boldsymbol{\theta}_\mathrm{max}$ obtained by physical reasoning.

V. Results

Three dehydration experimental data sets provide measurements for the outputs T_r, m_c, p_r, the input T_h and the disturbances T_c, T_a.

The experiments were carried out with different reactor set point temperatures to investigate the power connected to the mass transport from reactor to condenser. In the following,

TABLE II: Parameter from identification (id) with different data sets.

	id	$U_{\mathrm{hr}}/\mathrm{W}/(\mathrm{m}^2\,\mathrm{K})$	$U_{\mathrm{ra}}/\mathrm{W}/(\mathrm{m}^2\,\mathrm{K})$	$c_{\mathrm{cn,r}}/\mathrm{kJ}/\mathrm{K}$
①	E500, E470	111.80	2.76	14.80
②	E500, E430	143.86	5.52	17.09
③	E470, E430	233.29	10.61	24.48

the experiments are numbered with E for experiment and the desired set point temperature, which is $500\,^\circ\mathrm{C}$, $470\,^\circ\mathrm{C}$ and $430\,^\circ\mathrm{C}$. Therefore the experiments are labeled "E500", "E470" and "E430".

The measurement data is sampled with $\Delta t = 1\,\mathrm{s}$. Experiments E500, E470 and E430 include $N = 8135$, 8594 and 8384 time steps respectively. The model simulation in the identification optimization is carried out with $\Delta t_{\mathrm{sim}} = 0.1\,\mathrm{s}$, to guarantee the numerical stability of the conversion differential equation. To compare measurement and simulation, only every tenth time step of the simulation data is used. The times t_1 for opening of the condenser reactor connection for E500, E470, E430 are $t_1 = 889$, 947, $1108\,\mathrm{s}$, respectively.

The temperature of the thermostatic bath is set to $10\,^\circ\mathrm{C}$, the resulting temperature of the condenser water is nearly constant at $12.8{\pm}0.4\,^\circ\mathrm{C}$. Due to incomplete evacuation, the pressure in the condenser is slightly higher than the saturation vapor pressure that we assume for the condenser pressure. For all three experiments, the idealized condenser pressure via the magnus formula is approximately $1.5\,\mathrm{kPa}$, whereas the real condenser pressure lies between 3.0-$6.6\,\mathrm{kPa}$. As the reactor pressure is much higher at around $60\,\mathrm{kPa}/31\,\mathrm{kPa}/12\,\mathrm{kPa}$ for E500/E470/E430, we neglect this error. Especially for high reactor pressures, which are desirable due to the high reactor power, the modeling error of the condenser pressure is small and therefore neglectable. Physical deduction of the exact condenser pressure is prevented by the unknown amount of inert gases left after evacuation. Additionally, the pressure sensors have an accuracy of $\pm 0.6\,\mathrm{kPa}$. With more experimental data in the future, learning-based algorithms could help describe the relation between condenser temperature and pressure, and therefore further increase model accuracy.

The initial material mass for E500, E470, E430 is $4.966\,\mathrm{kg}$, $5.114\,\mathrm{kg}$, $4.903\,\mathrm{kg}$, with composition as stated in II-C.

The identification in the cross validation scheme was performed 100 times with random initial parameter values $\boldsymbol{\theta}_0$, to evaluate the convergence of the optimization. For all three identification variants, most of the identification runs converge to the same solution. The parameter combination with the lowest identification cost for every data set combination will be examined.

The resulting parameter combinations are shown in Tab. II, the corresponding evaluation of the root mean square error (RMSE) in Tab. III. The normalized RMSE is calculated by dividing the RMSE by the average value of the corresponding output, i.e. the average reactor temperature, condenser mass and reactor pressure.

Figure 4 shows the model simulation and measurements, as well as the heater temperature for every experiment. The numbers ①-③ in the legend refer to the numbering of the different cross validation parameter sets, cf. Tab. II. The validation data sets are marked with $*$.

TABLE III: Normalized RMSE and RMSE. The normalization is carried out with the average value of the corresponding output variable. The column id/val states whether the data set hast been used for identification (id) or validation (val).

			RMSE norm.			RMSE		
	Exp.	id/val	$T_{\mathrm{r}}/\%$	$m_{\mathrm{c}}/\%$	$p_{\mathrm{r}}/\%$	$T_{\mathrm{r}}/^\circ\mathrm{C}$	$m_{\mathrm{c}}/\mathrm{kg}$	$p_{\mathrm{r}}/\mathrm{kPa}$
①	E500	id	4.31	1.38	27.34	21.39	0.04	12.66
	E470	id	2.75	1.01	16.05	12.85	0.03	5.01
	E430	val	2.68	2.19	27.67	11.49	0.06	3.78
②	E500	id	4.48	1.39	27.82	22.23	0.04	12.88
	E470	val	3.13	0.60	16.80	14.64	0.02	5.25
	E430	id	3.37	1.70	26.22	14.42	0.05	3.58
③	E500	val	3.95	2.58	32.77	19.60	0.08	15.17
	E470	id	3.01	0.75	16.80	14.07	0.02	5.25
	E430	id	3.83	1.55	25.57	16.42	0.04	3.50

The parameter values in Tab. II are higher the lower the setpoint temperatures for the experiments in the identification, i.e. parameter set ① features the lowest values for all parameters and ③ the highest. For the dimension and relation between the parameters, no exact rule can be deduced. It can be observed the higher parameter U_{hr}, the higher the ratio to U_{ra} and the lower the ratio to $c_{\mathrm{cn,r}}$. In general, it is clear that with higher U_{hr} and therefore higher heat flow to the reactor, the other two parameter also have to increase, otherwise the reactor temperature and thus the conversion and pressure would be too high.

Since U_{hr} corresponds to the heat transfer from heater to reactor, its sensitivity is high when heater and reactor temperature are far apart, i.e. in the beginning of the experiment when the reactor heats up. Parameter $c_{\mathrm{cn,r}}$ has a damping effect on the reactor temperature, therefore its sensitivity is high for all setpoint changes through the heaters. Especially in the beginning of the experiment, the damping effect of $c_{\mathrm{cn,r}}$ can be observed. The sensitivity to parameter U_{ra}, corresponding to the heat loss to the ambiance, increases the higher the reactor temperature. If the reactor set point temperature is lower, e.g. for E430, different values and ratios between the parameters are optimal under the identification weights we chose. Therefore, the cross validation yields three distinct optimal parameter sets.

Figure 4 will now be examined in detail. The model fit for the reactor temperature (Figs. 4a-4c) is good for qualitative attributes like ripple and the temperature rise in the beginning. Overall, as the temperature fit has low weight in the identification problem, larger deviations occur. The weight was chosen low, as the temperature measurement in the middle of the reactor does not represent the average reactor temperature well. The current control logic and implementation for the heaters does not lead to a uniform heater temperature, but heaters are turned on and off separately. The control logic does not prevent one heating wire from switching off and the other heating wires compensating for it, as long as the reactor temperature meets the requirements and the heating wire temperatures are below their maximum value. The resulting temperature gradient in the reactor cannot be quantified, but the effect displays in

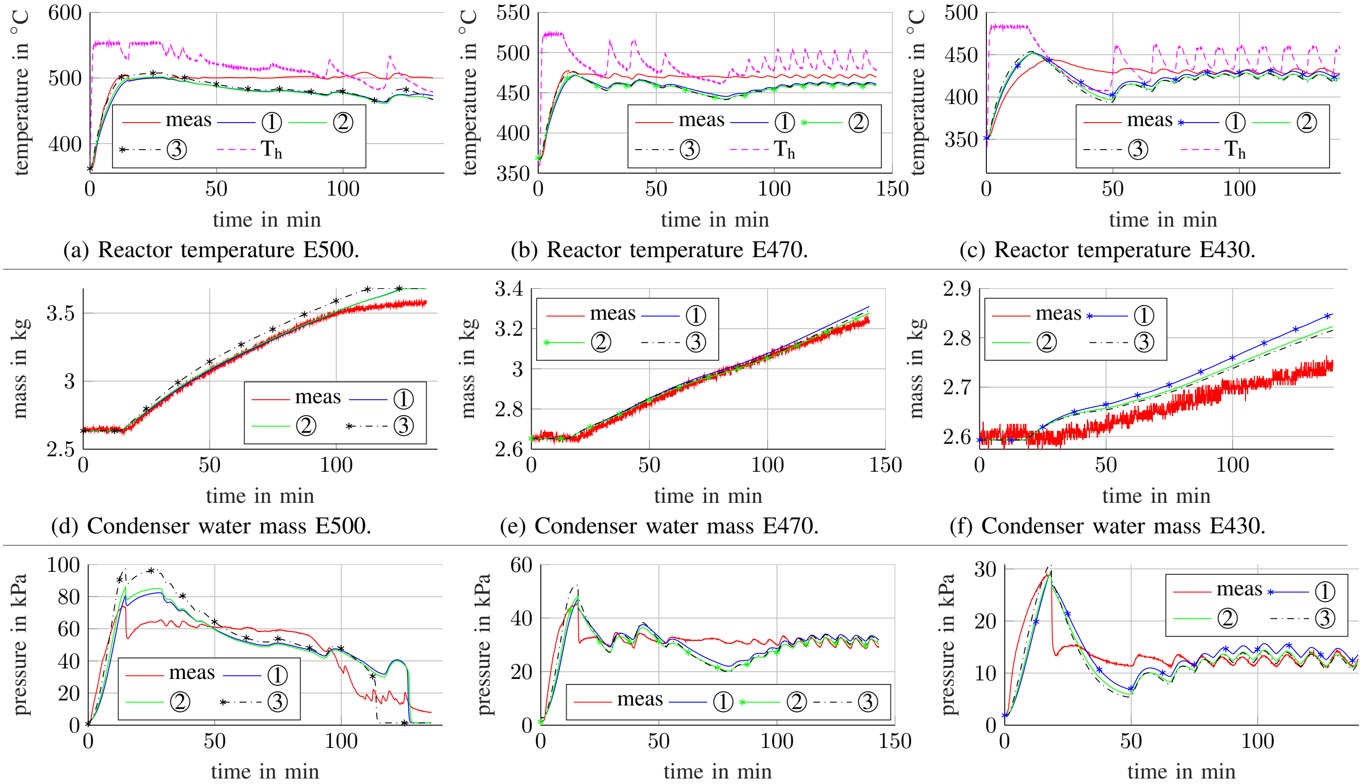

(a) Reactor temperature E500. (b) Reactor temperature E470. (c) Reactor temperature E430.

(d) Condenser water mass E500. (e) Condenser water mass E470. (f) Condenser water mass E430.

(g) Reactor pressure E500. (h) Reactor pressure E470. (i) Reactor pressure E430.

Fig. 4: Identified model outputs with parameter set that yields minimum identification cost. The parameter set for which the respective measurement was used for validation is marked by $*$.

the averaged heater temperature, that even falls below the measured reactor temperature from time to time.

The model displays a plausible average reactor temperature, which is not too far from the measured reactor temperature. Table III indicates 2.68-$4.48\,\%$ normalized RMSE for the reactor temperature.

The condenser mass, Figs. 4d-4f, exhibits the best model fit of the three outputs, having had the highest weight in the parameter identification optimization problem. For Figs. 4d and 4e, the model fits qualitatively and quantitatively very well with a normalized RMSE of 0.60-$1.39\,\%$. For 4f, deviations occur as soon as the connection between reactor and condenser is opened. The model error of the condenser pressure could lead to a higher water vapor mass flow, causing these errors. Also, the measurement accuracy of the fill level sensor of $0.0255\,\mathrm{kg}$ is only a slightly smaller than the model mismatch with an RMSE of 0.04-$0.06\,\mathrm{kg}$.

The reactor pressure is shown in Figs. 4g-4i. The model pressure is computed via the ideal gas law and therefore depends on the reactor temperature and the conversion. Overall, the qualitative pressure fit is good. The model displays the pressure drop when the reactor opens to the condenser as well as some ripple due to the rising and falling heater temperature. The pressure drop being less prominent in the model could be due to remaining inert gases in the real experiment that inherit different expansion properties than water vapor.

For E500, the real reaction slows down before full conversion is reached, which could be due to imperfect mixing and inhomogeneous heating. This leads to material deposits in colder reactor areas, which do not participate in the reaction. The model conversion from literature presumes ideal reaction conditions and therefore does not match in the end of the reaction. The model reaches full conversion, i.e. the maximum additional condenser water mass in Fig. 4d. As a result, since the reaction then does not produce any water vapor, the reactor pressure drops drastically in Fig. 4g. With more experimental data especially from experiments with high power and high conversion, a new conversion dynamic for the system could be identified, further improving model quality.

In [16], the authors calculate the effective heat transfer coefficient from the heated wall to the fluidized bed to be $156{\pm}16\,\mathrm{W/(m^2\,K)}$ during heating up and $243{\pm}52\,\mathrm{W/(m^2\,K)}$ for the dehydration process. Our model parameters ranges in a similar dimension, therefore are plausible. They are not equal, as the data used in [16] are different from the experimental data of this work. Furthermore, deviations occur because the parameters of our model not only describe physical properties, but other effects not covered by the model are lumped into them.

VI. Conclusion and Outlook

In this work, we set up a model of the dehydration in a novel heat storage system based on $Ca(OH)_2$. For three unknown parameters a parameter identification is performed via an optimization.

To allow for conclusions on the validity of the model, a cross validation scheme is applied to the three available measurement data sets, where the identification optimization problem is solved for two data sets and the third is used for model validation. All combinations of identification and validation data sets were evaluated, which yield different parameter solutions. As all parameters influence the thermal behavior of the reactor, the exact identification is challenging. The RMSE and its normalized version as well as the qualitative model behavior was evaluated.

Overall, parameter sets ① and ② display the best qualitative behavior, especially in Fig. 4d, and a good RMSE result. Parameter set ② yields the best RMSE result for the validation data, therefore this set is favored for further investigation of the system, e.g. system simulation at other set points and controller design for heaters and output power.

Possible steps to improve model quality are data driven learning of the relation between condenser temperature and pressure, as well as the setup of a new conversion dynamic based on more experimental data. Moreover, adaptive control with online parameter estimation to account for model uncertainties and different operating conditions will be investigated.

APPENDIX

The Tables IV and V list the symbols and parameters used in this work.

TABLE IV: Symbols and description.

Symbol	Description	Unit
A	area	m^2
c_p	molar heat capacity	$\mathrm{J/(mol\,K)}$
M	molar mass	$\mathrm{kg/mol}$
m	mass	kg
$\dot{m}$	mass flow	$\mathrm{kg/s}$
n	amount of substance	mol
$\dot{n}$	material flow	$\mathrm{mol/s}$
p	pressure	Pa
$\dot{Q}$	heat transfer	W
R_r	reaction rate	$\mathrm{mol/s}$
T	temperature	$^\circ\mathrm{C}$
U	thermal transmittance	$\mathrm{W/(m^2\,K)}$
X	conversion	$-$

TABLE V: Parameters and values. The upper range of parameters up to the division is from literature [18][19], the others are measured parameters or deduced from measurements.

Par.	Description	Value	Unit
$c_{\mathrm{p},1}$	molar heat capacity CaO	42.09	$\mathrm{J/(mol\,K)}$
$c_{\mathrm{p},2}$	molar heat capacity gas. water	38.47	$\mathrm{J/(mol\,K)}$
$c_{\mathrm{p},3}$	molar heat capacity $Ca(OH)_2$	87.45	$\mathrm{J/(mol\,K)}$
$H_{0,1}$	std. enthalpy of form. CaO	-635.09	$\mathrm{kJ/mol}$
$H_{0,2}$	std. enthalpy of form. gas. water	-241.82	$\mathrm{kJ/mol}$
$H_{0,3}$	std. enthalpy of form. $Ca(OH)_2$	-986.09	$\mathrm{kJ/mol}$
M_2	molar mass H_2O	$18.02 \cdot 10^{-3}$	$\mathrm{kg/mol}$
R	universal gas constant	8.314	$\mathrm{J/(mol\,K)}$
V_r	reactor volume	0.0157	m^3
A_hr	heat transfer area h to r	0.314	m^2
A_ra	heat transfer area r to amb.	0.314	m^2
η_rc	prop. fact. pres. dif. to mass flow	$2.93 \cdot 10^{-9}$	$\mathrm{kg/(s\,Pa)}$

ACKNOWLEDGMENT

This work was funded by the Deutsche Forschungsgemeinschaft (DFG, German Research Foundation) - Project-ID 279064222 - SFB 1244, A05 and the European Funds for Regional Development (EFRE Program) within the I-TESS project Project-ID EFRE-0801821.

REFERENCES

[1] International Energy Agency. Buildings, Paris. https://www.iea.org/energy-system/buildings, 2022. Accessed: 19.07.2023.

[2] United Nations Environment Programme. 2022 Global Status Report for Buildings and Construction: Towards a Zero-emission, Efficient and Resilient Buildings and Construction Sector. Nairobi., 2022.

[3] International Energy Agency. Heating, Paris. https://www.iea.org/energy-system/buildings/heating, 2022. Accessed: 19.07.2023.

[4] S. Lin, Y. Wang, and Y. Suzuki. High-Temperature CaO Hydration/$Ca(OH)_2$ Decomposition over a Multitude of Cycles. *Energy & Fuels*, 23(6):2855–2861, 2009.

[5] F. Schaube, L. Koch, A. Wörner, and H. Müller-Steinhagen. A thermodynamic and kinetic study of the de- and rehydration of $Ca(OH)_2$ at high H_2O partial pressures for thermo-chemical heat storage. *Thermochimica Acta*, 538:9–20, 2012.

[6] Y. A. Criado, M. Alonso, and J. C. Abanades. Kinetics of the CaO/$Ca(OH)_2$ Hydration/Dehydration Reaction for Thermochemical Energy Storage Applications. *Industrial & Engineering Chemistry Research*, 53(32):12594–12601, 2014.

[7] A. Gupta, P. D. Armatis, P. Sabharwall, B. M. Fronk, and V. Utgikar. Energy and exergy analysis of $Ca(OH)_2$/CaO dehydration-hydration chemical heat pump system: Effect of reaction temperature. *Journal of Energy Storage*, 39:102633, 2021.

[8] M. Schmidt and M. Linder. A Novel Thermochemical Long Term Storage Concept: Balance of Renewable Electricity and Heat Demand in Buildings. *Frontiers in Energy Research*, 8, 2020.

[9] Anja Rentz, Viktor Kühl, Venizelos E. Sourmelis T., Matthias Schmidt, Marc Linder, Oliver Sawodny, and Michael Böhm. Modeling and Identification of the Hydration Process in a CaO/Ca(OH)2-based Heat Storage System. *at - Automatisierungstechnik*, 71(8):584–598, 2023.

[10] B. J. Cott and S. Macchietto. Temperature control of exothermic batch reactors using generic model control. *Industrial & Engineering Chemistry Research*, 28(8):1177–1184, 1989.

[11] I. M. Mujtaba, N. Aziz, and M. A. Hussain. Neural Network Based Modelling and Control in Batch Reactor. *Chemical Engineering Research and Design*, 84(8):635–644, 2006.

[12] M. K. Tan, H. S. E. Chuo, H. J. Tham, Y. Y. Farm, and K. T. K. Teo. Genetic Algorithm Based Multivariable Control for Exothermic Batch Process. In *2012 Fourth International Conference on Computational Intelligence, Communication Systems and Networks (CICSyN 2012)*, pages 32–37, Piscataway, NJ, 2012. IEEE.

[13] H. Ogura, R. Shimojyo, H. Kage, Y. Matsuno, and A. S. Mujumdar. Simulation of Hydration/Dehydration of CaO/$Ca(OH)_2$ Chemical heat Pump Reactor for Cold/Heat Generation. *Drying Technology*, 17(7-8):1579–1592, 1999.

[14] Jun Yan, Lei Jiang, and Changying Zhao. Numerical Simulation of the $Ca(OH)_2$/CaO Thermochemical Heat Storage Process in an Internal Heating Fixed-Bed Reactor. *Sustainability*, 15(9):7141, 2023.

[15] S. Fujimoto, E. Bilgen, and H. Ogura. CaO/$Ca(OH)_2$ chemical heat pump system. *Energy Conversion and Management*, 43(7):947–960, 2002.

[16] K. Risthaus, M. Linder, and M. Schmidt. Experimental Investigation of a Novel Mechanically Fluidized Bed Reactor for Thermochemical Energy Storage with calcium hydroxide/calcium oxide. *Applied Energy*, 315:118976, 2022.

[17] WMO. *Guide to Meteorological Instruments and Methods of Observation*, volume 8 of *WMO*. World Meteorological Organization, Geneva, updated in 2017 edition, 2014.

[18] P. Linstrom. *NIST Chemistry WebBook, NIST Standard Reference Database 69*. National Institute of Standards and Technology, Gaithersburg MD, 1997.

[19] P. J. Mohr, B. N. Taylor, and D. B. Newell. CODATA recommended values of the fundamental physical constants: 2006. *Reviews of Modern Physics*, 80(2):633–730, 2008.